The $\tilde{X}^1A_1$ and $\tilde{a}^3B_2$ States of *o*-Benzyne: A Theoretical Characterization of Equilibrium Geometries, Harmonic Vibrational Frequencies, and the Singlet–Triplet Energy Gap

Andrew C. Scheiner,[†,⊥] Henry F. Schaefer III,[*,†] and Bowen Liu[‡]

Contribution from the Center for Computational Quantum Chemistry,[§] School of Chemical Sciences, University of Georgia, Athens, Georgia 30602, and IBM Research Division, Almaden Research Center, 650 Harry Road, San Jose, California 95120-6099.
Received December 7, 1987

Abstract: Using the methods of ab initio electronic structure theory, we have characterized the equilibrium geometries for the ground state and first excited state of the important organic reaction intermediate *o*-benzyne. Additionally, a complete set of harmonic vibrational frequencies and infrared absorption intensities has been determined at the ground-state equilibrium. Of great interest here is the character of the dehydrogenated C–C bond. Our best prediction for this bond distance is 1.25–1.26 Å, and for the harmonic vibrational frequency corresponding to the normal mode involving the stretch of this bond 1965–2010 cm^{-1}. This result is consistent with the gas-phase photodetachment study of Leopold, Miller, and Lineberger but is inconsistent with four independent matrix isolation infrared studies of *o*-benzyne. Several reassignments of observed fundamental vibrational frequencies are suggested. Also of interest is the energy gap between the $\tilde{X}^1A_1$ state and the low-lying $\tilde{a}^3B_2$ state which has been predicted herein to lie at 33.3 kcal/mol.

Much of the rich variety of chemical activity associated with benzene and substituted benzenes involves the reactive, yet isolable, intermediate *o*-benzyne or 1,2-dehydrobenzene, C_6H_4, illustrated below.[1]

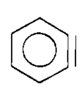

Perhaps the most well-known class of reactions involving this intermediate is the Diels–Alder addition. In fact, the Diels–Alder addition to furan, below, is considered a characteristic chemical test for the presence of *o*-benzyne in a reaction scheme.[1]

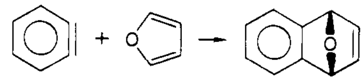

However, since the time of the original proposal of this species as an intermediate in the cis E2 elimination reaction of 1-chloro-[1-^{14}C]benzene with KNH_2 in 1953,[2] the direct physical identification and characterization of *o*-benzyne has proved difficult. Of inherent importance in the characterization of *o*-benzyne are the following. (1) What is the character of the C–C bond between the dehydrogenated carbon atoms? (2) Since the radical electrons at these two dehydrogenated carbon atoms can pair their spins in a parallel or an antiparallel sense, what is the energy gap between the $^1A_1$ ground state and the $\tilde{a}^3B_2$ state? (3) To what extent is the delocalized character of the π electrons of benzene perturbed by the dehydrogenation at adjacent carbon atoms?

At present our knowledge of the complete geometrical structure of *o*-benzyne is derived from the results of theoretical studies.[3–13] The most ambitious of these is the recent ab initio study of Hillier et al.[13] in which the equilibrium structure of the $\tilde{X}^1A_1$ state of *o*-benzyne was predicted by means of a two-configuration self-consistent-field wave function (TCSCF) obtained with a 6-31G* basis set which includes a set of polarizing d orbitals at each carbon center. It is interesting to note that the C–C bond distances determined by Hillier et al.[13] are nearly identical with those determined by radom et al.[12] who used the same TCSCF form of the wave function with the modest 3-21G basis set. These two studies (ref 12 and 13) demonstrated that both of the electron configurations illustrated in Figure 1 contribute significantly to the ground-state wave function of *o*-benzyne. Thus, when the equilibrium geometries reported therein are compared to single reference (based on the electron configuration with 10 doubly occupied a_1 molecular orbitals and seven doubly occupied b_2 MO's in Figure 1) ab initio structural predictions for the ground state of *o*-benzyne, substantial differences in the geometry are found.[5,7,8,11,12]

The infrared absorption studies of *o*-benzyne generated in low-temperature matrices[14–17] along with the recent study of the gas-phase electron photodetachment spectrum from the *o*-benzyne anion to the $\tilde{X}^1A_1$ and $\tilde{a}^3B_2$ states of the neutral by Leopold, Miller, and Lineberger (LML)[18] and the gas-phase microwave study by Brown, Godfrey, and Rodler[19] constitute the extent of the current,

† University of Georgia.
⊥ Present address: IBM Research Division, Almaden Research Center, 650 Harry Rd, San Jose, CA 95120-6099.
§ Contribution CCQC No. 6.
‡ IBM Research Division.

(1) Hoffmann, R. W. *Dehydrobenzene and Cycloalkynes*; Academic: New York, 1967.
(2) Roberts, J. D.; Simmons, H. E.; Carlsmith, L. A.; Vaughan, C. W. *J. Am. Chem. Soc.* **1953**, *75*, 3290.
(3) Coulson, C. A. *Chem. Soc., Spec. Publ.* **1958**, *12*, 85.
(4) Haselbach, E. *Helv. Chim. Acta* **1971**, *54*, 1987.
(5) Newton, M. D.; Fraenkel, H. A. *Chem. Phys. Lett.* **1973**, *18*, 244.
(6) Dewar, M. J. S.; Li, W.-K. *J. Am. Chem. Soc.* **1974**, *97*, 5569.
(7) Newton, M. D. In *Applicatons of Electronic Structure Theory* Schaefer, H. F., III, Ed.; Plenum: New York, 1977; p 223.
(8) Noell, J. O.; Newton, M. D. *J. Am. Chem. Soc.* **1979**, *101*, 51.
(9) Thiel, W. *J. Am. Chem. Soc.* **1981**, *103*, 1420.
(10) Dewar, M. J. S.; Ford, G. P.; Reynolds, C. H. *J. Am. Chem. Soc.* **1983**, *105*, 3162.
(11) Bock, C. W.; George, P.; Trachtman, M. *J. Phys. Chem.* **1984**, *88*, 1467.
(12) Radom, L.; Nobes, R. H.; Underwood, D. J.; Li, W.-K. *Pure Appl. Chem.* **1986**, *58*, 75.
(13) Hillier, I.; Vincent, M. A.; Guest, M. F.; von Niessen, W. *Chem. Phys. Lett.* **1987**, *134*, 403.
(14) Chapman, O. L.; Mattes, K.; McIntosh, C. L.; Pacansky, J.; Calder, G. V.; Orr, G. *J. Am. Chem. Soc.* **1973**, *95*, 6134. Chapman, O. L.; Chang, C.-C.; Kolc, J.; Rosenquist, N. R.; Tomioka, H. *J. Am. Chem. Soc.* **1975**, *97*, 6586.
(15) Dunkin, I. R.; MacDonald, J. G. *J. Chem. Soc., Chem. Commun.* **1979**, 772.
(16) Nam, H.-H.; Leroi, G. E. *J. Mol. Struct.* **1987**, *157*, 301.
(17) Wentrup, C.; Blanch, R.; Briehl, H.; Gross, G. *J. Am. Chem. Soc.* **1988**, *110*, 1874.
(18) Leopold, D. G.; Miller, A. E. S.; Lineberger, W. C. *J. Am. Chem. Soc.* **1986**, *108*, 1379.
(19) Brown, R. D.; Godfrey, P. D.; Rodler, M. *J. Am. Chem. Soc.* **1986**, *108*, 1296.

0002-7863/89/1511-3118$01.50/0

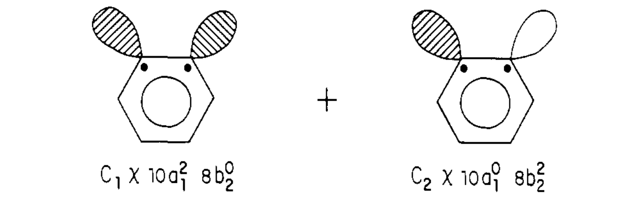

Figure 1. The two electronic configurations used in the TCSCF description of the $\tilde{X}^1A_1$ state of *o*-benzyne. $\chi \equiv 1b_2^2 1a_1^2 2a_1^2 2b_2^2 3a_1^2 3b_2^2 4a_1^2 4b_2^2 5a_1^2 6a_1^2 5b_2^2 7a_1^2 6b_2^2 8a_1^2 7b_2^2 9a_1^2 1b_1^2 2b_1^2 1a_2^2$.

direct spectroscopic characterization of *o*-benzyne. While complete spectroscopic determination of the ground-state geometry or vibrational spectrum has not yet been reported, the assignments of several ground-state fundamental vibrational frequencies have played an important role in the development of our current understanding of the bonding in this intermediate. In comparing the reported assignments for the interesting and important (in terms of the bonding across the "triple" C–C bond) dehydrogenated C–C stretching fundamental, however, one finds that the characterization of this mode remains unsettled. While the four matrix IR experiments[14-17] and two normal coordinate analyses based on the matrix bands[20,21] concur that this dehydrogenated stretching mode absorbs at 2080–2091 cm^{-1} (characteristic of an acetylenic type C–C bond), LML assign a feature at 1860 cm^{-1} in their gas-phase photodetachment spectrum to this same vibrational mode.[18] A C–C stretching frequency of this value is more characteristic of a C–C bond intermediate between a typical double bond and a typical triple bond. It seems unlikely that such a large discrepancy (220 cm^{-1}) could be due to the different environments in which these spectra were recorded. Thus there is a fundamental conflict between the two experimental values for this most important vibrational frequency of *o*-benzyne. Also of interest here are two theoretical studies of the vibrational spectrum of *o*-benzyne. Radom et al. determined a harmonic frequency of 2209 cm^{-1} using an ab initio 3-21G SCF wave function.[12] These authors further scaled this value by 0.9 (to estimate the effects of an improved theoretical description of the wave function and anharmonicity) yielding 1988 cm^{-1}. An earlier MNDO study of Dewar, Ford, and Rzepa[22] found the dehydrogenated C–C stretching frequency at 2042 cm^{-1}. Both of these predictions lie intermediate between the matrix IR and the gas-phase photodetachment assignments.

With regard to the singlet–triplet energy gap, LML have determined a value of 37.7 (6) kcal/mol.[18] This result is considerably greater than Noell and Newton's theoretical prediction of 28 kcal/mol.[8]

We have carried out an ab initio theoretical study of *o*-benzyne in order to further investigate these questions and apparent inconsistencies which are crucial to the understanding and characterization of this important intermediate. Specifically, fully optimized geometries for the $\tilde{X}^1A_1$ and $\tilde{a}^3B_2$ states have been determined (and thus the energy gap between these two low-lying states). Additionally, the harmonic vibrational spectrum of the ground state has been studied. In what follows we present (1) a description of our theoretical methods, (2) results and discussion for the ground-state geometry, (3) results and discussion for the ground-state vibrational spectrum, (4) results and discussion for the $\tilde{a}^3B_2$ state and the singlet–triplet energy gap, (5) concluding remarks.

Theoretical Method

As stated above, recent ab initio results have demonstrated that the $\tilde{X}^1A_1$ equilibrium geometry of *o*-benzyne depends critically on the form of the ground-state wave function.[12,13] We have investigated this further by optimizing the ground-state geometry employing (i) a single-configuration SCF wave function based on the antisymmetrized determinant

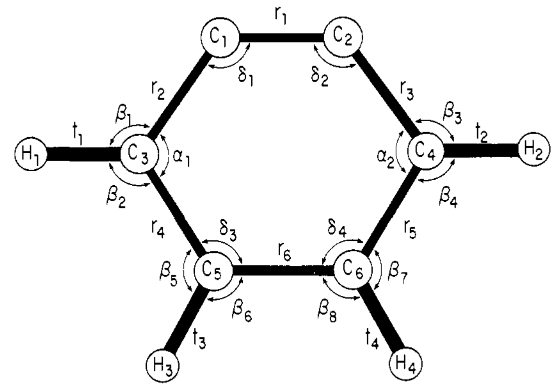

Figure 2. Specification of the equilibrium geometry of $\tilde{X}^1A_1$ *o*-benzyne.

$\chi\ 10a_1^2$ illustrated in Figure 1, (ii) a two-configurational SCF (TCSCF) wave function based on a linear combination of the two determinants illustrated in Figure 1, and (iii) a wave function incorporating the effects of dynamic electron correlation through second-order in many-electron perturbation theory (MP2) based on the $\chi\ 10a_1^2 8b_2^0$ SCF reference determinant. All electrons and all orbitals were active in the MP2 wave function. The $\tilde{a}^3B_2$ state of *o*-benzyne was studied using standard open-shell restricted Hartree–Fock (RHF) theoretical methods.

The one-electron atomic basis employed for the present study was the standard Dunning double-ζ contraction[23] of Huzinaga's primitive Gaussian orbitals[24] (with the hydrogen *s* functions scaled by 1.2) augmented with a single set of polarization functions at each of the atomic centers (DZ + P basis set). The polarization orbital exponents were chosen as $\alpha_d(C) = 0.75$ and $\alpha_p(H) = 0.75$. This DZ + P basis set totaled 116 atomic functions and is thus significantly larger than those used in previous ab initio theoretical studies.

Harmonic vibrational analyses have been carried out at the DZ + P SCF, TCSCF, and MP2 ground-state geometries yielding harmonic frequencies and (for the SCF and MP2 methods only) infrared absorption intensities for both C_6H_4 and C_6D_4. In the case of the SCF method, force constants and dipole derivatives were evaluated by analytic differentiation of the energy with respect to nuclear displacement and electric field.[25] The TCSCF and MP2 force constants and the MP2 dipole derivatives were determined via finite differences of analytically evaluated energy gradients and dipole moments.

For the TCSCF force constant evaluation, analytic TCSCF gradients at finite displacements (0.005 Å in bond distances and 0.005 radian in bond angles) from the TCSCF equilibrium geometry were evaluated for each of the symmetrized internal coordinates defined in Table IV. In total, 33 displacements on the ground-state surface were required ($2 \times 9a_1 + 4a_2 + 3b_1 + 8b_2$). A further difficulty arose because the eight displacements which transform as b_2 take the nuclear framework into a geometry in which the only remaining symmetry element is the molecular plane. In such a C_s point group, the two active TCSCF orbitals ($10a_1$ and $8b_2$ within the full C_{2v} symmetry at the equilibrium geometry) both transform as a'. Consequently, the excited-state TCSCF method of Fitzgerald and Schaefer[26] was required for these b_2 displacements because standard TCSCF techniques break down in such cases. The MP2 force constants and IR intensities were evaluated via Cartesian displacements of 0.005 Å.

In order to investigate the effect of valence dynamic electron correlation on the theoretical singlet–triplet energy gap (ΔE_{S-T}), we have evaluated the $\tilde{X}^1A_1$ and $\tilde{a}^3B_2$ energies using configuration interaction wave functions including all single and double excitations (with the exclusion of the six carbon 1s-like orbitals and the corresponding high-energy virtual MOs) out of the SCF and TCSCF reference wave functions (CISD). These CISD energies were determined at the corresponding SCF and TCSCF equilibrium geometries. Davidson's correction for disconnected quadruple excitations[27] was appended to each of the CISD energies.

Throughout the present study, all $^3B_2$ open-shell RHF and all $^1A_1$ TCSCF and TC-CISD studies were carried out at the Center for Computational Quantum Chemistry using the PSI quantum chemistry programs. All $^1A_1$ single determinant based SCF, CISD, and MP2 studies

(20) Laing, J. W.; Berry, R. S. *J. Am. Chem. Soc.* **1976**, *98*, 660.
(21) Nam, H.-H.; Leroi, G. E. *Spectrochimica Acta, Part A* **1985**, *41*, 67.
(22) Dewar, M. J. S.; Ford, G. P.; Rzepa, H. S. *J. Mol. Struct.* **1979**, *51*, 275.
(23) Dunning, T. H. *J. Chem. Phys.* **1970**, *53*, 2823.
(24) Huzinaga, S. *J. Chem. Phys.* **1965**, *42*, 1293.
(25) Osamura, Y.; Yamaguchi, Y.; Saxe, P.; Vincent, M. A.; Gaw, J. F.; Schaefer, H. F. *Chem. Phys.* **1982**, *72*, 131.
(26) Fitzgerald, G.; Schaefer, H. F. *J. Chem. Phys.* **1985**, *83*, 1162.
(27) Davidson, E. R. In *The World of Quantum Chemistry*; Daudel, R., Pullman, B., Eds.; Reidel: Dodrecht, 1974; pp 17–30.

were carried out at the IBM Almaden Research Center using the GAUSSIAN 86 program.[28]

Results and Discussion

I. $\tilde{X}^1A_1$ Geometry. Table I summarizes our results for the equilibrium geometry of the $\tilde{X}^1A_1$ state of *o*-benzyne. Also included are the results of other recent theoretical studies. The coordinates used to specify the geometry are defined in Figure 2. We have grouped the results into three categories: (i) single-configuration SCF theory (based on $\chi\ 10a_1^2$ as illustrated in Figure 1) which takes no electron correlation into account, (ii) two-configuration SCF theory which allows for contributions to the ground state from both electron configurations illustrated in Figure 1, and (iii) theories incorporating dynamic electron correlation (DEC).

The qualitative picture of the *o*-benzyne ring geometry which emerges from Table I is clear. The C_1–C_2 bond distance, r_1, contracts upon dehydrogenation relative to benzene ($r_{C\text{-}C}$ = 1.388 Å, 6-31G* SCF),[11] and in progressing around the ring from the dehydrogenated C–C bond, there is a stepwise lengthening of the C–C bond distances, $r_1 \ll r_2 < r_4 < r_6$. Note that in all cases while $r_2 < r_4 < r_6$, these three distances are only slightly perturbed from the parent benzene. As detailed by Bock, George, and Trachtman,[11] using comparisons of their 6-31G SCF results to analogous results for the bond distances in 1-buten-3-yne, *trans*-1,3-butadiene, and benzene, a preservation of the aromatic character of benzene in *o*-benzyne is clearly apparent. In the case of the MP2 results and especially the TCSCF results, even less deviation from benzene-like hexagonality (relative to the SCF *o*-benzyne geometries) is observed.

Based on the results in Table I, the quantitative picture of the $\tilde{X}^1A_1$ *o*-benzyne geometry appears not yet completely resolved. In particular, the C_1–C_2 bond distance shows quite a bit of variation with respect to the theoretical method employed. Using a simple one-configuration wave function to describe this state, one finds the C_1–C_2 distance to range from 1.22 to 1.23 Å. However, by including contributions from both the bonding ($\chi\ 10a_1^2$) and antibonding ($\chi\ 8b_2^2$) configurations illustrated in Figure 1, this distance increases to 1.26 Å. Within such a TCSCF description, we find (as did Hillier et al.)[13] that the coefficient for the $\chi\ 10a_1^2$ determinant is 0.94 (89% bonding) and that for the $\chi\ 8b_2^2$ determinant is 0.33 (11% antibonding). In terms of the GVB overlap analysis discussed by Noell and Newton,[8] the overlap for the nonorthogonal GVB orbitals based on our DZ + P TCSCF wave function is 0.480. This suggests a slightly greater diradical character than their 4-31G TCSCF result of 0.508.[8] This may be a result of their constraining the TCSCF geometry at the 4-31G SCF equilibrium in which the C_1–C_2 bond is a short 1.226 Å.[7] Finally, if one includes dynamic electron correlation, one finds that the dehydrogenated C–C bond distance lengthens further to our DZ + P MP2 value of 1.275 Å.

Another interesting observation regarding the triple bond vs diradical nature of the C_1–C_2 interaction is that while the long MP2 C_1–C_2 distance might suggest that the MP2 wave function incorporates a greater amount of diradical character than does the TCSCF wave function, a closer inspection of the ring geometries suggests otherwise. First of all, correlating the electrons through second-order in perturbation theory elongates all of the C–C bonds (relative to the SCF independent electron reference results) albeit to a lesser extent than the C_1–C_2 bond. More importantly, when comparing the DZ + P SCF, TCSCF, and MP2 equilibrium C_3–C_1–C_2 angles (δ_1 in Figure 2), one finds that TCSCF results in the most bending (δ_1 = 125.7°) adjacent to the "triple-bond" and thus presumably the greatest diradical contribution to the wave function. The MP2 description results in a somewhat more linear (less diradical) geometry (δ_1 = 126.6°), and the single determinant description yields the least bent structure of all (δ_1 = 127.5°).

Given the variation in Table I, where does theory stand with respect to prediction of the equilibrium $\tilde{X}^1A_1$ geometry of *o*-benzyne? In ref 11 Bock, George, and Trachtman have attempted to address this question by correcting their 6-31G SCF and 6-31G* SCF bond distances using known theory versus experiment discrepancies for acetylene, ethylene, and benzene. This procedure yielded r_1 = 1.240 Å, r_2 = 1.393 Å, r_3 = 1.402 Å, r_4 = 1.412 Å, δ_1 = 127°, α_1 = 110°, δ_3 = 123°, and $t_1 = t_3$ = 1.081 Å. This is a reasonable procedure in lieu of more definitive theoretical or experimental results; however, such predictions may not always be reliable, particularly in this case where neither acetylene, ethylene, nor benzene has such a large diradical contribution to the ground-state wave function. We believe our DZ + P TCSCF results to be a more realistic picture of the ground-state equilibrium geometry. Going beyond the TCSCF description to include the effects of dynamic electron correlation out of the TCSCF reference wave function will most probably reduce the C_1–C_2 bond distance somewhat ($\simeq$0.005–0.015 Å), so that our best prediction for this distance is in the range 1.25–1.26 Å. This is characteristic of a C–C bond intermediate between a typical C–C triple bond and a typical C–C double bond.

II. $\tilde{X}^1A_1$ Vibrational Spectrum. In Tables II and III we present our DZ + P SCF, TCSCF, and MP2 theoretical results for the ground-state harmonic frequencies (and where available, infrared absorption intensities) of the 24 normal modes of C_6H_4 and C_6D_4. Each normal mode is classified by its irreducible representation within the C_{2v} point group and characterized by its potential energy distribution based on the 24 symmetrized internal coordinates defined in Table IV. This potential energy distribution (PED) based on the diagonal elements of the symmetrized internal coordinate force constant matrix is defined for a given normal mode n as

$$F_k(\%) \equiv [\delta S_k{}^n]^2 F_{kk} / \sum_{i=1}^{3N-6} [\delta S_i{}^n]^2 F_{ii}$$

where $F_k(\%)$ is the percentage energy contribution to normal mode n from displacement along symmetrized internal coordinate S_k, and F_{ii} are the diagonal elements of the force constant matrix. In Tables II and III, the sign of F_k indicates the phase of the displacement relative to the defined symmetrized internal coordinates (Table IV). Based on the present theoretical results, we have assigned the bands observed in the experimental spectra, and these assignments, which will be dicussed below, are reflected in the two right-most columns of the tables.

Focusing our attention first on the totally symmetric mode corresponding to the dehydrogenated C–C stretch, not surprisingly, we find a rather large variation with the level of theory: SCF ω_0 = 2184 cm^{-1}, TCSCF ω_0 = 1922 cm^{-1}, and MP2 ω_0 = 1931 cm^{-1} for C_6H_4, and correspondingly, 2175, 1912, and 1924 cm^{-1} for C_6D_4. For reasons to be given, the theoretical limit of the true harmonic frequency for this mode most probably lies below the SCF result and above the TCSCF and MP2 values. however, since investigating the effects of a more complete basis and a more complete treatment of electron correlation on the *o*-benzyne harmonic force field is currently impractical, we have taken as an approximate model for this mode the C–C stretch in acetylene and have made use of the recent results of Simandiras et al.[29] to estimate our basis set and electron correlation deficiencies.

As reported by Simandiras et al.[29] the acetylene DZ + P SCF harmonic C–C stretching frequency overestimates the experimental harmonic by 9.7% (2207 versus 2011 cm^{-1}).[30] Conversely, the DZ + P MP2 result of Simandiras et al. (1956 cm^{-1}) underestimates experiment by 2.2%. Applying the above two corrections to our DZ + P SCF and DZ + P MP2 C_6H_4 harmonic C_1–C_2 stretching frequencies, respectively, yields 1990 cm^{-1} (corrected DZ + P SCF) and 1985 cm^{-1} (corrected DZ + P MP2). Associating a 20-cm^{-1} uncertainty with these corrected values, we predict that the true harmonic frequency for the dehydrogenated

(28) Frisch, M.; Binkley, J.; Schlegel, H.; Raghavachari, K.; Melius, C.; Martin, R.; Stewart, J.; Bobrowicz, F.; Rohlfing, C.; Kahn, L.; DeFrees, D.; Seeger, R.; Whiteside, R.; Fox, D.; Fluder, E.; Pople, J. GAUSSIAN 86; Carnegie-Mellon Quantum Chemistry Publishing Unit: Pittsburgh, PA, 1984.

(29) Simandiras, E. D.; Rice, J. E.; Lee, T. J.; Amos, R. D.; Handy, N. C. *J. Chem. Phys.* **1988**, *88*, 3187.

(30) Strey, G.; Mills, I. M. *J. Mol. Spectrosc.* 1976, *59*, 103.

Table I. Equilibrium Geometry of the Ground State of *o*-Benzyne[a]

	SCF			TCSCF			DEC
	6-31G[b]	6-31G*[b]	DZ+P[c]	3-21G[d]	6-31G*[e]	DZ+P[c]	DZ+P MP2[c]
r_1	1.232	1.223	1.225	1.261	1.260	1.263	1.275
r_2	1.385	1.382	1.389	1.382	1.383	1.388	1.398
r_4	1.398	1.391	1.395	1.389	1.389	1.393	1.413
r_6	1.411	1.410	1.415	1.404	1.404	1.409	1.417
t_1	1.069	1.073	1.076		1.073	1.076	1.088
t_3	1.073	1.076	1.079		1.076	1.078	1.090
α_1	110.2	110.2	109.9		112.4	112.3	110.7
β_1	126.8	126.9	127.1		125.3	125.4	126.8
β_5	118.9	118.9	119.0		119.3	119.2	118.5

[a] Bond distances in Å; angles in deg. Refer to Figure 2 for definition of coordinates. DEC = dynamic electron correlation. [b] Reference 11. [c] Present work. [d] Reference 12. [e] Reference 13.

Table II. *o*-Benzyne Vibrational Spectrum[a]

	DZ+P SCF			DZ+P TCSCF		DZ+P MP2			mode description	experimental ν_0	
	ω_0	IR int	PED[b]	ω_0	PED[b]	ω_0	IR int	PED[b]		I	II
a_1	3401	6.8	$F_5(92)$ $F_6(7)$	3398	$F_5(87)$ $F_6(12)$	3270	6.8	$F_5(79)$ $F_6(20)$	C–H str	3088	
a_1	3367	12.3	$F_6(92)$ $F_5(-7)$	3371	$F_6(87)$ $F_5(-13)$	3247	1.8	$F_6(79)$ $F_5(-21)$	C–H str		
a_1	2184	1.7	$F_1(82)$ $F_3(-10)$	1922	$F_1(68)$ $F_3(-15)$	1931	2.0	$F_1(76)$ $F_3(-19)$	C_1–C_2 str	2082, 2084, 2085	1860
a_1	1589	0.0	$F_9(32)$ $F_2(28)$ $F_8(24)$	1589	$F_8(31)$ $F_9(29)$ $F_2(23)$	1506	1.0	$F_2(46)$ $F_9(24)$ $F_4(-18)$	ring str + H wag	1596, 1598, 1607	
a_1	1390	0.0	$F_8(40)$ $F_4(32)$ $F_9(-10)$	1388	$F_8(33)$ $F_4(30)$ $F_9(-13)$	1390	0.6	$F_8(48)$ $F_4(34)$ $F_3(-14)$	ring str + H wag	1395	
a_1	1230	0.9	$F_9(50)$ $F_4(25)$ $F_2(-14)$	1225	$F_9(44)$ $F_4(27)$ $F_2(-18)$	1167	0.9	$F_9(69)$ $F_8(-18)$ $F_2(-7)$	ring str + H wag		
a_1	1078	33.0	$F_3(71)$ $F_2(16)$ $F_4(-9)$	1094	$F_3(68)$ $F_4(-15)$ $F_8(9)$	1065	20.7	$F_3(69)$ $F_1(19)$ $F_8(8)$	ring str	1055, 1056, 1053	1044
a_1	1066	5.7	$F_4(42)$ $F_2(39)$ $F_8(-15)$	1077	$F_2(51)$ $F_4(29)$ $F_8(-10)$	1003	4.3	$F_4(42)$ $F_2(41)$ $F_8(-13)$	ring str + H wag	1038, 1039	
a_1	663	0.6	$F_7(92)$	650	$F_7(92)$	606	0.0	$F_7(92)$	$C_{1(2)}$–$C_{3(4)}$–$C_{5(6)}$ bend		605
a_2	1083	0.0	$F_{12}(68)$ $F_{11}(-24)$ $F_{10}(4)$	1089	$F_{12}(70)$ $F_{11}(-22)$ $F_{10}(4)$	885	0.0	$F_{12}(51)$ $F_{11}(-45)$ $F_{10}(4)$	H wag		
a_2	954	0.0	$F_{11}(60)$ $F_{12}(38)$	959	$F_{11}(64)$ $F_{12}(33)$	823	0.0	$F_{12}(60)$ $F_{11}(34)$ $F_{10}(6)$	H wag		
a_2	626	0.0	$F_{13}(58)$ $F_{11}(-20)$ $F_{10}(13)$	684	$F_{13}(82)$ $F_{11}(-13)$ $F_{12}(6)$	611	0.0	$F_{13}(74)$ $F_{11}(-14)$ $F_{12}(12)$	ring torsion		
a_2	435	0.0	$F_{10}(50)$ $F_{13}(-46)$	485	$F_{10}(64)$ $F_{13}(-34)$	468	0.0	$F_{10}(71)$ $F_{13}(-25)$	ring torsion		
b_1	1036	0.0	$F_{15}(53)$ $F_{16}(-40)$ $F_{14}(7)$	1042	$F_{15}(56)$ $F_{16}(-38)$ $F_{14}(7)$	851	0.5	$F_{15}(47)$ $F_{16}(-46)$ $F_{14}(7)$	H wag		
b_1	825	102.5	$F_{16}(49)$ $F_{15}(47)$	820	$F_{16}(51)$ $F_{15}(47)$	726	90.0	$F_{15}(54)$ $F_{16}(42)$	H wag	739, 743, 735	
b_1	425	9.6	$F_{14}(84)$ $F_{16}(-15)$	441	$F_{14}(87)$ $F_{16}(-12)$	386	7.0	$F_{14}(83)$ $F_{16}(-16)$	ring torsion		
b_2	3398	27.6	$F_{19}(95)$	3395	$F_{19}(93)$ $F_{20}(5)$	3266	14.6	$F_{19}(91)$ $F_{20}(8)$	C–H str		
b_2	3350	4.7	$F_{20}(96)$	3354	$F_{20}(94)$ $F_{19}(-5)$	3230	0.2	$F_{20}(91)$ $F_{19}(-8)$	C–H str		
b_2	1632	22.1	$F_{18}(54)$ $F_{24}(-20)$ $F_{17}(13)$ $F_{23}(11)$	1674	$F_{18}(49)$ $F_{17}(22)$ $F_{23}(13)$ $F_{24}(-13)$	1505	0.1	$F_{18}(46)$ $F_{17}(27)$ $F_{23}(12)$ $F_{24}(-11)$	ring str + H wag	1627	
b_2	1526	3.1	$F_{17}(48)$ $F_{24}(18)$ $F_{23}(13)$ $F_{21}(9)$	1544	$F_{17}(40)$ $F_{24}(38)$ $F_{23}(10)$ $F_{21}(9)$	1419	11.3	$F_{17}(46)$ $F_{24}(33)$ $F_{21}(11)$ $F_{23}(5)$	ring str + H wag + $C_{1(2)}$–$C_{3(4)}$–$C_{5(6)}$ bend	1448, 1451	
b_2	1355	0.0	$F_{17}(42)$ $F_{23}(-42)$ $F_{21}(11)$ $F_{24}(-5)$	1349	$F_{23}(46)$ $F_{17}(-41)$ $F_{21}(-9)$	1269	0.0	$F_{23}(56)$ $F_{17}(-29)$ $F_{24}(7)$ $F_{21}(-7)$	ring str + H wag + $C_{1(2)}$–$C_{3(4)}$–$C_{5(6)}$ bend	1355	
b_2	1198	2.0	$F_{18}(38)$ $F_{24}(36)$ $F_{21}(-17)$ $F_{23}(-16)$	1201	$F_{18}(39)$ $F_{24}(24)$ $F_{21}(-17)$ $F_{23}(-13)$	1116	1.3	$F_{18}(38)$ $F_{24}(26)$ $F_{21}(-17)$ $F_{23}(-14)$	ring str + H wag + $C_{1(2)}$–$C_{3(4)}$–$C_{5(6)}$ bend		
b_2	890	34.0	$F_{21}(86)$ $F_{22}(-7)$	958	$F_{21}(78)$ $F_{22}(-20)$	875	9.2	$F_{21}(77)$ $F_{22}(-21)$	$C_{1(2)}$–$C_{3(4)}$–$C_{5(6)}$ bend	848, 847, 849	
b_2	303	188.9	$F_{22}(60)$ $F_{21}(-38)$	585	$F_{22}(81)$ $F_{21}(-12)$	589	6.9	$F_{22}(83)$ $F_{21}(-16)$	$C_{3(4)}$–$C_{1(2)}$–$C_{2(1)}$ bend	470, 472, 469	

[a] Frequencies in cm^{-1}; infrared intensities in km/mol. Expt I = matrix IR (ref 16 and references therein). Expt II = gas-phase electron photodetachment (ref 18). [b] Dominant contributions to diagonal potential energy distribution; sign indicates phase of displacement relative to defined symmetrized internal coordinates (see Table IV).

Table III. Perdeutero-*o*-benzyne Vibrational Spectrum[a]

	DZ+P SCF			DZ+P TCSCF		DZ+P MP2			mode description	experimental ν_0	
	ω_0	IR int	PED[b]	ω_0	PED[b]	ω_0	IR int	PED[b]		I	II
a_1	2524	5.2	$F_5(85)\ F_6(10)$	2520	$F_5(77)\ F_6(19)$	2425	5.8	$F_5(70)\ F_6(26)$	C–D str	2293	
a_1	2490	5.3	$F_6(86)\ F_5(-10)$	2493	$F_6(77)\ F_5(-19)$	2400	0.1	$F_6(70)\ F_5(-26)$	C–D str		
a_1	2175	2.4	$F_1(83)\ F_3(-9)$	1912	$F_1(71)\ F_3(-14)$	1924	1.4	$F_1(77)\ F_3(-18)$	C_1–C_2 str	2093	1860
a_1	1473	1.8	$F_2(47)\ F_9(16)\ F_4(-10)$	1464	$F_2(44)\ F_1(-20)\ F_9(15)$	1465	1.6	$F_2(50)\ F_4-(34)\ F_9(9)$	ring str + D wag		
a_1	1266	4.5	$F_4(54)\ F_8(22)\ F_3(-19)$	1285	$F_4(52)\ F_3(-22)\ F_8(17)$	1273	3.7	$F_3(33)\ F_8(-29)\ F_4(-26)$	ring str + D wag		
a_1	1055	13.0	$F_3(60)\ F_2(27)$	1058	$F_3(56)\ F_2(26)\ F_4(7)$	1007	5.5	$F_3(42)\ F_4(22)\ F_2(19)$	ring str	1108	980
a_1	899	0.2	$F_9(73)\ F_2(-15)\ F_8(-8)$	902	$F_9(76)\ F_2(-14)\ F_8(-7)$	840	0.3	$F_9(79)\ F_8(-14)\ F_2(-5)$	D wag	882	
a_1	855	13.6	$F_8(60)\ F_4(-18)\ F_3(10)$	862	$F_8(63)\ F_4(-15)\ F_3(9)$	804	9.7	$F_8(60)\ F_2(-13)\ F_4(-12)$	D wag + ring str	792	
a_1	642	0.5	$F_7(89)\ F_9(-7)$	630	$F_7(90)\ F_9(-7)$	586	0.0	$F_7(89)\ F_9(-8)$	$C_{1(2)}$–$C_{3(4)}$–$C_{5(6)}$ bend		585
a_2	894	0.0	$F_{12}(66)\ F_{11}(-14)\ F_{10}(10)$	899	$F_{12}(64)\ F_{11}(-16)\ F_{13}(12)$	690	0.0	$F_{12}(64)\ F_{11}(-14)\ F_{10}(12)$	D wag		
a_2	738	0.0	$F_{11}(81)\ F_{12}(16)$	744	$F_{11}(72)\ F_{12}(17)$	646	0.0	$F_{11}(72)\ F_{12}(18)$	D wag		
a_2	539	0.0	$F_{13}(84)\ F_{11}(-16)$	616	$F_{13}(86)\ F_{10}(-10)$	586	0.0	$F_{13}(83)\ F_{10}(-11)$	ring torsion		
a_2	429	0.0	$F_{10}(54)\ F_{13}(-44)$	456	$F_{10}(72)\ F_{13}(-28)$	434	0.0	$F_{10}(78)\ F_{13}(-21)$	ring torsion		
b_1	841	0.3	$F_{15}(54)\ F_{16}(-29)\ F_{14}(17)$	845	$F_{15}(55)\ F_{16}(-28)\ F_{14}(17)$	685	0.3	$F_{15}(52)\ F_{16}(-29)\ F_{14}(19)$	D wag + ring torsion		
b_1	638	48.3	$F_{16}(58)\ F_{15}(35)$	631	$F_{16}(57)\ F_{15}(37)$	564	43.1	$F_{16}(58)\ F_{15}(34)$	D wag	616	
b_1	368	10.5	$F_{14}(82)\ F_{16}(-17)$	384	$F_{14}(86)\ F_{16}(-13)$	334	8.3	$F_{14}(81)\ F_{16}(-17)$	ring torsion		
b_2	2517	26.4	$F_{19}(85)\ F_{20}(7)$	2516	$F_{19}(83)\ F_{20}(9)$	2420	11.3	$F_{19}(83)\ F_{20}(10)$	C–D str		
b_2	2472	0.7	$F_{20}(89)\ F_{19}(-8)$	2476	$F_{20}(86)\ F_{19}(-10)$	2380	0.1	$F_{20}(85)\ F_{19}(-11)$	C–D str		
b_2	1576	11.0	$F_{18}(52)\ F_{17}(34)\ F_{23}(7)$	1625	$F_{18}(47)\ F_{17}(38)\ F_{23}(7)$	1472	0.6	$F_{17}(47)\ F_{18}(39)\ F_{23}(6)$	ring str	1483	
b_2	1410	1.7	$F_{17}(53)\ F_{21}(18)\ F_{18}(-13)\ F_{24}(12)$	1413	$F_{17}(48)\ F_{18}(-17)\ F_{21}(17)\ F_{24}(15)$	1317	4.2	$F_{17}(42)\ F_{18}(-24)\ F_{21}(18)\ F_{24}(14)$	ring str + H wag + $C_{1(2)}$–$C_{3(4)}$–$C_{5(6)}$ bend	1293	
b_2	1070	0.2	$F_{23}(49)\ F_{24}(36)\ F_{17}(-8)$	1068	$F_{23}(48)\ F_{24}(32)\ F_{17}(-10)$	988	0.5	$F_{23}(54)\ F_{24}(-35)\ F_{17}(-6)$	D wag	1029	
b_2	918	1.2	$F_{21}(50)\ F_{24}(-18)\ F_{23}(17)$	941	$F_{21}(75)\ F_{22}(-14)$	868	1.9	$F_{21}(71)\ F_{22}(-13)\ F_{24}(-6)$	C–C–C bend		
b_2	835	34.8	$F_{21}(63)\ F_{23}(-14)\ F_{24}(11)\ F_{22}(-6)$	890	$F_{21}(26)\ F_{24}(24)\ F_{23}(-23)\ F_{22}(-16)$	817	9.6	$F_{21}(36)\ F_{22}(-21)\ F_{24}(18)\ F_{23}(-17)$	C–C–C bend + D wag	730	
b_2	301	186.1	$F_{22}(60)\ F_{21}(-37)$	576	$F_{22}(81)\ F_{21}(-17)$	580	5.8	$F_{22}(83)\ F_{21}(-15)$	$C_{3(4)}$–$C_{1(2)}$–$C_{2(1)}$ bend	471	

[a] Frequencies in cm^{-1}; infrared intensities in km/mol. Expt I = matrix IR (ref 15). Expt II = gas-phase electron photodetachment (ref 16). [b] Dominant contributions to diagonal potential energy distribution; sign indicates phase of displacement relative to defined symmetrized internal coordinates (see Table IV).

Table IV. Symmetrized Internal Coordinates for *o*-Benzyne in C_{2v} Symmetry[a]

a_1	$Q_1 = \Delta r_1$	a_1	$Q_9 = (1/\sqrt{2})(\Delta\beta_5 - \Delta\beta_6 + \Delta\beta_7 - \Delta\beta_8)$	b_2	$Q_{17} = (1/\sqrt{2})(\Delta r_3 - \Delta r_2)$
a_1	$Q_2 = \Delta r_6$	a_2	$Q_{10} = \Delta\tau_3$	b_2	$Q_{18} = (1/\sqrt{2})(\Delta r_4 - \Delta r_5)$
a_1	$Q_3 = (1/\sqrt{2})(\Delta r_2 + \Delta r_3)$	a_2	$Q_{11} = (1/\sqrt{2})(\Delta\kappa_1 - \Delta\kappa_4)$	b_2	$Q_{19} = (1/\sqrt{2})(\Delta t_1 - \Delta t_2)$
a_1	$Q_4 = (1/\sqrt{2})(\Delta r_4 + \Delta r_5)$	a_2	$Q_{12} = (1/\sqrt{2})(\Delta\kappa_2 - \Delta\kappa_3)$	b_2	$Q_{20} = (1/\sqrt{2})(\Delta t_3 - \Delta t_4)$
a_1	$Q_5 = (1/\sqrt{2})(\Delta t_1 + \Delta t_2)$	a_2	$Q_{13} = (1/\sqrt{2})(\Delta\tau_1 + \Delta\tau_2)$	b_2	$Q_{21} = (1/\sqrt{2})(\Delta\alpha_1 - \Delta\alpha_2)$
a_1	$Q_6 = (1/\sqrt{2})(\Delta t_3 + \Delta t_4)$	b_1	$Q_{14} = (1/\sqrt{2})(\Delta\tau_1 - \Delta\tau_2)$	b_2	$Q_{22} = (1/\sqrt{2})(\Delta\delta_1 - \Delta\delta_2)$
a_1	$Q_7 = (1/\sqrt{2})(\Delta\alpha_1 + \Delta\alpha_2)$	b_1	$Q_{15} = (1/\sqrt{2})(\Delta\kappa_1 + \Delta\kappa_4)$	b_2	$Q_{23} = (1/\sqrt{2})(\Delta\beta_1 - \Delta\beta_2 - \Delta\beta_3 + \Delta\beta_4)$
a_1	$Q_8 = (1/\sqrt{2})(\Delta\beta_1 - \Delta\beta_2 + \Delta\beta_3 - \Delta\beta_4)$	b_1	$Q_{16} = (1/\sqrt{2})(\Delta\kappa_2 + \Delta\kappa_3)$	b_2	$Q_{24} = (1/\sqrt{2})(\Delta\beta_5 - \Delta\beta_6 - \Delta\beta_7 + \Delta\beta_8)$

[a] Refer to Figure 2 for definition of internal coordinates. κ_1: H_2–C_4 out of C_2–C_4–C_6 plane angle. κ_2: H_4–C_6 out of C_4–C_6–C_5 plane angle. κ_3: H_3–C_5 out of C_6–C_5–C_3 plane angle. κ_4: H_1–C_3 out of C_5–C_3–C_1 plane angle. τ_1: torsional angle between C_5–C_3–C_1 and C_3–C_1–C_2 planes. τ_2: torsional angle between C_6–C_4–C_2 and C_4–C_2–C_1 planes. τ_3: torsional angle between C_5–C_1–C_6 and C_1–C_6–C_2 planes.

C–C stretch of *o*-benzyne lies in the range 1965–2010 cm^{-1}.

With respect to the experimental assignments of this fundamental frequency, first of all, it is difficult to incorporate the matrix IR assignment at 2080–2085 cm^{-1} [14-17] into a consistent picture with our predicted harmonic range. Any anharmonicity associated with this mode would most probably yield a fundamental of lower frequency than the associated harmonic, and frequency shifts due to matrix effects are typically less than 5 cm^{-1} in magnitude. Furthermore, since we have based our prediction of the harmonic vibrational frequency of this mode on corrections to the SCF and MP2 results, neither of which includes diradical contributions in the reference determinant, any additional diradical character neglected by these two theories would tend to reduce the harmonic value further. This is evidenced by our TCSCF result of 1922 cm^{-1}. A second inconsistency with the matrix IR assignment is found by examining the frequency shift of this mode in the C_6D_4 isomer. With the three theoretical methods, we find a red shift of the harmonic upon deuteration of 7–10 cm^{-1}, whereas the IR band identified in the matrix as the C_1–C_2 stretch is blue shifted by 9 cm^{-1} upon deuteration.[15] In light of these inconsistencies, it may be prudent to consider the question of whether the band observed at 2080–2085 cm^{-1} in the low-temperature matrix experiments arises from *o*-benzyne or from a secondary product of the matrix photolysis. Concerning this, Wentrup et al. have shown that at least one additional photolysis product (cyclopentadienylideneketene) also absorbs at 2080–2090 cm^{-1}.[17]

Through a Franck–Condon anaylsis of the vibronic transition profile from $C_6H_4^-$ ($C_6D_4^-$) to the $\tilde{X}^1A_1$ state of neutral C_6H_4 (C_6D_4) [with a dominant progression of 605 cm^{-1} (585 cm^{-1}) and partially resolved features corresponding to a second progression of 1040 cm^{-1} (980 cm^{-1}), discussed further below], LML extracted a third fundamental frequency at 1860 cm^{-1} (1860 cm^{-1}).[18] The 1860-cm^{-1} fundamental was assigned to the dehydrogenated C–C stretch. Although the procedure used to obtain this value was indirect and is referred to by LML as "somewhat inferential", such an assignment appears remarkably consistent with the present theoretical prediction. While no attempt has been made in the present study to account for anharmonicity in the *o*-benzyne force field, there appears to be no other theoretical harmonic frequency to which the 1860-cm^{-1} band could reasonably be assigned. Finally, while no frequency shift was observed by LML upon deuteration, they associate a 15-cm^{-1} uncertainty with both the C_6H_4 and C_6D_4 bands at 1860 cm^{-1}. Thus the 7–10-cm^{-1} red shift predicted herein may be beyond the precision of the photodetachment experiment.

To conclude the discussion of the dehydrogenated C–C stretch, we note that two normal coordinate analyses of the vibrational spectrum of *o*-benzyne have been reported.[20,21] In each of these studies an initial guess at the force constant matrix was systematically modified to best fit the observed bands in the matrix IR spectra. The bands at 2085 cm^{-1} (C_6H_4) and 2093 cm^{-1} (C_6D_4) are thus, not surprisingly, reproduced by these analyses. Interestingly, however, both of the normal coordinate analyses report a red shift of this mode upon deuteration in conflict with the matrix data but in accord with the present study. A second interesting point (first noted by LML)[18] is that the earlier analysis of Laing and Berry[20] did predict a frequency at 1856 cm^{-1} which was assigned to a mode by b_2 symmetry. While the more recent analysis of Nam and Leroi[21] finds no bands between 1700 and 2000 cm^{-1}, such an 1856-cm^{-1} fundamental would correspond nicely with the 1860-cm^{-1} gas-phase interval extracted from the photodetachment spectrum, and thus, with the harmonic value predicted herein. Finally, it should be noted that the best-fit frequencies obtained from both of the normal coordinate analyses used geometries which differ substantially from our predicted range for r_1 (1.25–1.26 Å). The Laing and Berry geometry, which was obtained from a best fit to the matrix bands, contains an very long C_1–C_2 distance of 1.344 Å. Conversely, Nam and Leroi fixed the *o*-benzyne geometry (at the 4-31G SCF equilibrium[7]) with a short C_1–C_2 distance of 1.226 Å.

We turn next to the remainder of the *o*-benzyne vibrational spectrum. According to our MP2 intensity profile, the most intense band in the IR spectrum should correspond to the b_1 H wag with a DZ + P MP2 harmonic frequency of 726 cm^{-1}. Based on this result, we assign the strong absorption originally observed by Chapman et al.[14a] at 735 cm^{-1} to this b_1 mode. Furthermore, we concur with Radom et al.[12] that the strong band originally observed by Chapman et al.[14a] at 849 cm^{-1} is best assigned to the b_2 α_1–α_2 (see Figure 2) bend with DZ + P MP2 ω_0 = 875 cm^{-1} and intensity = 9.2 km/mol. Such an assignment is in disaccord with the assignments of Nam and Leroi[16] based on the normal coordinate analysis[21] in which observed bands have been assigned to each of the three modes which transform as b_1. Based on the present results, it appears that the low-frequency b_1 ring torsion (which we find to have a reasonably strong IR intensity) has not yet been observed. Additionally, as noted in Table II, we have assigned the moderately intense band first observed at 1038 cm^{-1} [14a] to the low-frequency a_1 mixed ring stretch + H wag for which DZ + P MP2 (SCF) predicts ω_0 = 1003 (1066) cm^{-1} and an intensity of 4.3 (5.7) km/mol. This assignment is in disaccord with those of both Radom et al.[12] and Nam and Leroi[16] who assigned this band to the high-frequency a_2 H wag (IR inactive) and the high-frequency b_1 H wag [DZ + P MP2 (SCF) intensity = 0.5 (0.3) km/mol], respectively.

The assignments for many of the C_6D_4 matrix IR bands in Table III are also in disaccord with earlier assignments.[12,21] In particular, we have again assigned only one matrix IR band to a b_1 normal mode (the very intense D wag) in contrast to the normal mode analysis in which all three b_1 modes were assigned.[21] Additionally, the bands at 1483 and 1293 cm^{-1} which were previously assigned to a_1 modes[21] appear better assigned to b_2 modes. Conversely, the bands at 1108 and 822 cm^{-1} have been reassigned from b_2[21] to a_1.

The major vibronic progression in the C_6H_4 (C_6D_4) photodetachment spectrum at 605 (585) cm^{-1} was assigned to the lowest frequency totally symmetric ring bending mode, and the partially resolved features at 1040 (980) cm^{-1} were assigned to the totally symmetric ring stretch (at 1053–1056 cm^{-1} in the C_6H_4 matrix).[17] Our results are certainly consistent with such assignments and Tables II and III reflect this. As noted by LML,[18] the two normal coordinate analyses found the low-frequency a_1 ring bending mode to be less stiff with frequencies of 395[21] and 471 cm^{-1}.[20]

In summary, we have attempted to provide a reasonable fit to the observed bands with our theoretical harmonic frequencies and intensities. While this is the most rigorous ab initio study of *o*-benzyne to date, we should be aware of limitations and potential problems. First, there is no guarantee that all of the bands attributed to *o*-benzyne in the matrix are, in fact, attributable to *o*-benzyne. Thus one or more of the matrix IR bands in Tables II and III may arise from a secondary photolysis product or intermediate. Specifically, the feature at 2082–2085 cm^{-1} does not appear to be either the dehydrogenated C–C stretch or any of the other fundamental vibrational frequencies of *o*-benzyne. Second, no attempt has been made to investigate the effects of anharmonicity on the theoretical force field. For this, higher order derivatives of the potential surface would be required. Third, it is generally believed that a more complete basis set (than DZ + P) is needed for reliable predictions of infrared absorption intensities. Thus we have used the theoretical intensities as a qualitative guide for our assignments. For example, based on our intensity data, the absorption corresponding to the low-frequency b_1 H wag should be a strong band in the IR spectrum. On the other hand, it is difficult to base an assignment solely on the theoretical intensities for the two high-frequency mixed b_2 modes which appear to swap intensity upon improvement of the wave function from SCF to MP2. Lastly, it must be kept in mind that the frequencies and, in particular, the intensities may be perturbed in the matrices relative to the corresponding gas-phase values.

III. $\tilde{a}^3B_2$ Equilibrium Geometry and the Singlet–Triplet Energy Gap. Table V presents our results for the DZ + P SCF equilibrium geometry of the $\tilde{a}^3B_2$ state of *o*-benzyne. As evidenced by the C–C bond distances, the triplet equilibrium corresponds to a nearly hexagonal structure. This result is ce-tainly reasonable in that, to a first approximation, one has minimally perturbed the elec-

Table V. The DZ+P SCF Equilibrium Geometry of $\tilde{a}\ ^3B_2$ *o*-Benzyne[a]

r_1	1.391 Å	t_1	1.077 Å
r_2	1.377 Å	t_3	1.077 Å
r_4	1.399 Å	α_1	118.3°
r_6	1.388 Å	β_1	120.7°
		β_5	120.6°

[a] Refer to Figure 2 for definition of coordinates.

Table VI. The Singlet–Triplet Energy Gap of *o*-Benzyne ($E^1{}_{A_1} - E^3{}_{B_2}$)[a]

	$\tilde{X}\ ^1A_1$ total energy	$\Delta E_{S\text{-}T}$
DZ+P SCF($^1A_1$)/SCF($^3B_2$)	−229.422 192	−2.9
DZ+P CISD($^1A_1$)/CISD($^3B_2$)	−230.075 497	17.0
+ Davidson correction	−230.227 426	48.3
DZ+P TCSCF($^1A_1$)/SCF($^3B_2$)	−229.470 872	27.7
DZ+P TC-CISD($^1A_1$)/CISD($^3B_2$)	−230.099 808	32.2
+ Davidson correction	−230.203 444	33.3
photoelectron spectrum[b]		37.7 (6)

[a] Total $^1A_1$ state energies are expressed in hartrees, and $\Delta E_{S\text{-}T}$ is expressed in kcal/mol. All CI energies were evaluated at the SCF stationary points. [b] Reference 18.

tronic structure of benzene by dehydrogenating two adjacent carbon centers such that the remaining unpaired electrons have parallel spin, occupying the bonding a_1 orbital and the antibonding b_2 orbital equally. In the case of the ground state, the two radical electrons are allowed to occupy the same spatial molecular orbital. As discussed above, the $\tilde{X}^1A_1$ C_1–C_2 distance (and thus the character of the unpaired electrons) is particulary sensitive to the form of the wave function used to describe the ground state; however, in all cases there is additional bonding across C_1–C_2, and the σ framework of the ring must distort somewhat in order to accommodate this.

Our theoretical results for the singlet–triplet energy gap, $\Delta E_{S\text{-}T}$, are compared with the experimental result of LML in Table VI. For purposes of an energetic reference, the total electronic energies of the singlet state as predicted by the six theoretical methods are included in Table VI. The inherent inadequacies of a single-determinant description of the $^1A_1$ state become strikingly obvious from the first three rows of Table VI. In fact, based on a simple SCF description, the $^3B_2$ state is incorrectly predicted to be the ground state of *o*-benzyne. A CISD description, while incorporating some diradical contribution to the singlet state, is still unable to compensate for the poor SCF single reference description. Furthermore, the Davidson correction is clearly inappropriate for the $^1A_1$ CISD wave function based on the single $\chi\ 10a_1^2$ determinant because of the important second configuration ($\chi\ 8b_2^2$). This is borne out by the relatively small CISD reference coefficient (0.876), and thus, the unrealistically large energy lowering of the singlet state. By using a TC–CISD description of the ground state, however, one obtains a much more balanced description of the two low-lying states. A recent systematic study of the electron affinities of O, F, and CH_2 using multireference CI methods demonstrated that one can obtain a balanced treatment of a pair of electronic states by choosing the reference spaces for the two states such that the sum of the squares of the CI coefficients corresponding to the reference configurations are comparable for the two states under consideration.[31] In the case of the $\tilde{X}^1A_1$ versus $\tilde{a}^3B_2$ states of *o*-benzyne, the square of the $^3B_2$ CISD reference coefficient is $(0.914)^2 = 0.835$ which is equal to the $^1A_1$ TC–CISD result of $(0.875)^2 + (-0.263)^2 = 0.835$. In contrast for the single reference based CISD description of the $^1A_1$ state, $(C_0)^2 = (0.876)^2 = 0.767$. Finally, we note that in the case of the TC–CISD singlet-state wave function, the Davidson correction is appropriate (the next largest CI coefficient is 0.047). In lieu of a more rigorous treatment of the effects of higher excitations, this theory yields our best prediction for the singlet–triplet energy gap of 33.3 kcal/mol (within 4.5 kcal/mol of the gap determined from the photodetachment spectrum[18]). To obtain further improvements in the theoretical accuracy, significant expansion of the basis set would most probably be needed.

(31) Noro, T.; Yoshimine, M. private communication.

Concluding Remarks

Based on our predictions for the equilibrium geometry and harmonic vibrational frequencies of the $\tilde{X}^1A_1$ state of *o*-benzyne, the dehydrogenated C–C bond is best described as intermediate between a C–C double bond and a C–C triple bond. It appears that the diradical contributions to the ground-state wave function are important in obtaining a realistic geometric characterization of this intermediate. As reported previously,[11] we have found that the hexagonal structure (reflecting the extent of π electron delocalization about the six-membered ring) of benzene is retained to a great extent by *o*-benzyne. In the case of the $\tilde{a}^3B_2$ state, there is very little deviation from hexagonality.

With respect to the vibrational spectrum of *o*-benzyne, our 1965–2010-cm^{-1} prediction for the harmonic vibrational frequency corresponding primarily to the dehydrogenated C–C stretch cannot be fit into a consistent picture with the body of matrix IR spectra for which a band in the range 2080–2085 cm^{-1} has been assigned to this same C_1–C_2 stretching fundamental.[14-17] Furthermore, based on the results of the present study, we find no other harmonic vibrational frequency which could be reasonably assigned to such matrix observations. We have explored a variety of isotopic substitutions about the *o*-benzyne ring with the hope of finding a particular isotope for which the IR absorption intensity of this important mode could be substantially improved; however, no such isotope was discovered. Several other bands observed in the C_6H_4 and C_6D_4 matrix have been given new assignments based on our theoretical results. In particular, it appears that only one out-of-plane mode has been observed. Our results are in accord with the three fundamental frequency assignments based on a Franck–Condon analysis of the photoelectron transition from $\tilde{X}^2B_2$ $C_6H_4^-$ (C_6D_4) to $\tilde{X}^1A_1$ C_6H_4 (C_6D_4).[18] In particular, based on the present theoretical study, the indirectly observed 1860-cm^{-1} band appears to be a more reasonable value for the dehydrogenated C–C stretch than that obtained from the matrix spectra.[14-17]

Our prediction for the singlet–triplet energy gap of 33.3 kcal/mol is in accord with the 37.7 kcal/mol result obtained from the photodetachment spectrum of Leopold, Miller, and Lineberger.[18] This quantity is quite sensitive to the level of theory applied. Based on the present ab initio study, a two-configuration based approach is required for a meaningful description of the ground-state wave function.

Acknowledgment. The CCQC research was supported by the U.S. National Science Foundation, Grant CHE-8718469. A.C.S. and H.F.S. thank Professors W. C. Lineberger and Wesley D. Allen for helpful discussions. A.C.S. also is grateful to Dr. M. D. Miller, Dr. J. Pacansky, and Professor O. L. Chapman for fruitful discussions and for providing a copy of the original matrix spectrum of *o*-benzyne.